

# Stellar Evolution Research in the Far-IR in the *AKARI* Era and Beyond

TOSHIYA UETA<sup>1</sup>

<sup>1</sup>*Department of Physics and Astronomy, University of Denver, Denver, CO 80208, USA*

## ABSTRACT

At the turn of the 21<sup>st</sup> century, we enjoyed a *renaissance* of far-IR astronomy because of the coming of the next generation of far-IR satellites, *Spitzer*, *AKARI*, and *Herschel*. Here, we quickly summarize outcomes of the stellar evolution research done using far-IR data taken these space telescopes, especially those that are based on imaging of the evolved star circumstellar shells. Also, we briefly outline what to be done using the next generation of far-IR telescopes.

**Keywords:** infrared: stars, stars: AGB and post-AGB, circumstellar matter, stars: mass-loss, stars: winds, outflows, planetary nebulae: general

## 1. INTRODUCTION

### 1.1. Dusty Stellar Mass Loss and Resulting Circumstellar Envelopes

Stars lose the surface material to the surrounding space over the course of their evolution in one way or another. High-mass stars (of  $> 8\text{--}10 M_{\odot}$ ) expel most of their mass in an explosion at the end of their lives as supernovae, while low- to intermediate-mass stars (of  $< 8\text{--}10 M_{\odot}$ ) lose their masses in an often steady mass-loss that wither them away into white dwarfs. However, we have not completely understood how stellar mass loss happens as a natural consequence of first principles of physics. Sedlmayr (1994) estimated that more than 80 % of the matter annually injected into the interstellar medium (ISM) originated from low- to intermediate-mass stars (of from about 0.8 to  $8\text{--}10 M_{\odot}$  initial mass). These stars are numerous and experience copious mass loss at the rate of  $10^{-7}\text{--}10^{-4} M_{\odot} \text{ yr}^{-1}$  during the late stages of evolution, especially during the asymptotic giant branch (AGB) phase (cf., Herwig 2005; Iben 2012; Karakas & Lattanzio 2014).

This heavy mass loss by evolved stars not only affects the ISM environments, i.e., the chemical evolution of galaxies, but also impacts critically the evolution of stars themselves, i.e., the fate of these stars. For example, mass loss can exhibit temporal variations because of the alternative burning of hydrogen and helium in distinct internal layers via “thermal pulses” (Iben 1981), while a dramatic increase of the rate of mass loss toward the end of the AGB phase called the “superwind” (Renzini 1981) can remove the bulk of the surface material from the star thereby terminating the AGB evolution. Mass loss processes including these specific phenomena are supposedly natural consequences of internal evolution, while the course of the internal evolution would presumably be influenced critically by these very mass loss processes. Because of this inner coupling and the resulting complications, no theoretical description of mass loss has ever been fully developed to date, and the existing models of the late stages of stellar evolution are heavily dependent on the choice of a particular mass-loss prescription adopted (e.g., Karakas & Lattanzio 2014).

Nonetheless, the matter ejected from the stellar surface during the AGB phase would always develop a circumstellar envelope (CSE), regardless of the true mass loss mechanisms. The CSE of AGB stars, especially of young AGB stars, is generally spherically symmetric presumably reflecting the spherical nature of mass loss during the early AGB phase. The classic example of it is seen in the concentric shells around a well-known carbon star, IRC 10216 (Figure 1, left; Mauron & Huggins 1999). When the AGB mass loss is terminated at the end of the AGB phase, the CSE becomes physically detached from the central star and begins to coast away. A number of imaging surveys of such post-AGB CSEs (also known as proto-planetary nebulae, or PPNe; Kwok 1993; Van Winckel 2003) has been conducted both in the optical (probing the dust distribution of PPNe indirectly via dust-scattered star light; Ueta et al. 2000; Sahai et al. 2007; Siódmiak et al. 2008) and mid-IR (probing the dust distribution directly via thermal dust emission; Meixner et al. 1999; Lagadec et al. 2011). As a result of these surveys, the evolved star CSEs are generally considered to become largely axisymmetric by the end of the AGB phase, because of the emergence of the central dust torus whose optical thickness essentially determines the CSE morphology (Ueta 2002; Meixner et al. 2002). The archetypical examples of the bifurcated PPN morphologies are represented by the bipolar structure of the Egg Nebula (Figure 1, middle; Sahai et al. 1998) and the elliptical structure of IRAS 07134+1005 (Figure 1, right; Meixner et al. 2004).

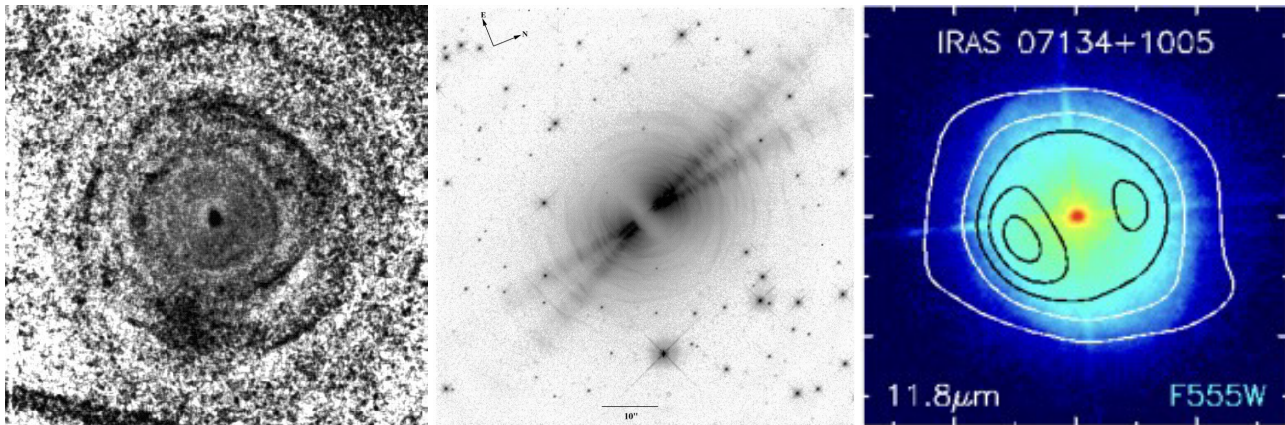


**Figure 1.** The CSE structure transition from spherical to axisymmetric in the late stages of stellar evolution. **Left:** Ground-based  $B+V$  image of the carbon-rich AGB CSE, IRC 10+216, in the  $131'' \times 131''$  field, showing concentric structures in the CSE (Mauron & Huggins 1999). **Middle:** HST V (WFPC2/F606W) image of the bipolar PPN, Egg Nebula, in the  $74'' \times 74''$  field, showing the equatorial optically-thick region as the dust lane separating the bipolar nebulae (Sahai et al. 1998). **Right:** HST V (WFPC2/F555W) color-image and ground-based  $11.8 \mu\text{m}$  contours of the PPN, IRAS 07134+1005, in the  $7'' \times 7''$  field, showing the central optically-thin dust torus at the edge-on orientation embedded within the elliptical reflection nebula (Meixner et al. 2004)

### 1.2. The Onset of Structure Development in the AGB Winds

However, still critically lacking is the direct observational evidence of the CSE structure development in the AGB mass loss, especially during the epoch of the CSE structure transition from spherical to axisymmetric (Figure 1). The past investigation using thermal dust emission in the mid-IR probed the innermost regions of PPNe, which are concerned with only the latest AGB mass loss histories (Meixner et al. 1999; Ueta et al. 2001; Gledhill & Yates 2003; Lagadec et al. 2011). To capture the onset of the CSE structure transition, therefore, we must probe the outer regions of the evolved star CSEs, in which this structural transition is represented as morphological variations in the dust density distributions. While the bulk of the circumstellar matter is in the form of neutral (atomic and molecular) gas in such evolved star CSEs (e.g., Knapp & Morris 1985; Castro-Carrizo et al. 2010), molecules are usually photo-dissociated by the interstellar radiation field (ISRF) in the outer parts of the CSEs (e.g., Meixner et al. 1998). Even though most recent ALMA observations have revealed many spiral structures in the AGB CSEs suggesting the active role that the central binary system plays in modulating the rate of mass loss (e.g., Maercker et al. 2012), interferometric observations by ALMA tend to resolve out large-scale structures in the outer CSEs that are critical to probe the AGB mass loss history into more distant past.

Hence, dust emission remains to be a viable tracer of the outer reaches of the evolved star CSEs, i.e., of older mass-loss histories including the onset of the structural transition in the AGB dusty stellar winds. The ISRF heats the outermost regions of the CSEs and keeps the temperature of dust in these regions around a few tens K, making far-IR imaging the most effective method to probe the outer CSEs. Such extended evolved star CSEs were indeed detected first by the pioneering work (e.g., Hacking et al. 1985; Stencel et al. 1988; Hawkins & Zuckerman 1991; Young et al. 1993a,b) done with the *Infrared Astronomical Satellite* (*IRAS*; Neugebauer et al. 1984). However, low spatial resolution of *IRAS* precluded any detailed examinations of the CSE structures. With high-resolution image processing of *IRAS* data, the structures of a few CSEs were recognized (e.g., Waters et al. 1994; Izumiura et al. 1997; Hashimoto et al. 1998). Subsequent studies using the *Infrared Space Observatory* (*ISO*; Kessler et al. 1996) confirmed the existence of large extended AGB CSEs by a series of work via direct imaging (Izumiura et al. 1996; Izumiura & Hashimoto 1998; Hashimoto & Izumiura 1998).

### 1.3. The Renaissance of Far-IR Astronomy at the Turn of the 21<sup>st</sup> Century

At the turn of the 21<sup>st</sup> century, there was a *renaissance* of far-IR astronomy with the coming of the next generation of space telescopes launched successively – the *Spitzer Space Telescope* (*Spitzer*; Werner et al. 2004) in 2003 by the US National Aeronautics and Space Administration, the *AKARI* infrared astronomical satellite (*AKARI*; Murakami et al. 2007) in 2006 by the Institute of Space and Aeronautical Science (ISAS) of the Japan Aerospace Exploration Agency (JAXA), and the *Herschel Space Observatory* (*Herschel*; Pilbratt et al. 2010) in 2009 by the European Space Agency. These new opportunities permitted us to probe the outer regions of the evolved star CSEs at better sensitivities and spatial resolution than the preceding studies with *IRAS* and *ISO*.

As one of the trio of far-IR space telescopes, from its launch in 2006 to the end of its mission in 2011, *AKARI* surveyed the entire sky in six bands in the wavelength range between 9 and  $160 \mu\text{m}$  for the first time since *IRAS* (Neugebauer et al. 1984) and conducted nearly 20,000 pointed observations of specific targets to provide deeper images and spectroscopic data from near- to far-IR wavelength ranges. Below, we will briefly summarize a select few topics of stellar evolution research done with the far-IR data provided by *AKARI* and other telescopes and allude to remaining major issues to be addressed by the future generation of far-IR telescopes.

## 2. THE DETECTION OF THE AGB CSE-ISM INTERFACE REGION IN THE FAR-IR

The CSE-ISM interface region around high-mass stars was known to be bright in the far-IR from *IRAS* all-sky observations (van Buren & McCray 1988; van Buren et al. 1995; Noriega-Crespo et al. 1997a). One of the most notable *IRAS* results was the arc structure for Betelgeuse (Stencel et al. 1988; Noriega-Crespo et al. 1997b; Figure 2a), which was followed up two decades later with *AKARI* (Ueta et al. 2008; Figure 2b) and *Herschel* (Decin et al. 2012; Figure 2c). From the initial discovery, the characteristic arc structure was recognized as the natural consequence of interactions between the stellar winds and the surrounding ISM (Stencel et al. 1988). With highly-processed images aided by theoretical calculations, Noriega-Crespo et al. (1997b) concluded that the arc structure was confined by the ram pressure of the ISM.

Ueta et al. (2008) fit the apparent arc shape to the stellar wind bow shock cone structure analytically derived by Wilkin (1996), using the higher spatial-resolution *AKARI* scan maps. Also with the most recent astrometric solution at the time for the star provided by Harper et al. (2008), the fit yielded the 3-D orientation of the stellar wind bow shock cone with respect to us, as well as associated quantities that characterized the ISM dynamics local to the object. Apparently, there had been an outflow of  $n_{\text{H}} = 1.5\text{--}1.9\text{ cm}^{-3}$  at  $v_{\text{ISM}} \sim 11\text{ km s}^{-1}$  emanating from the Orion OB1 association (from the location of the Orion Nebula to the location of Betelgeuse, almost into the NNE). Betelgeuse was found to have been traversing across this outflow at  $v_* = 40n_{\text{H}}^{-1/2}\text{ km s}^{-1}$  (i.e., about  $30\text{ km s}^{-1}$  given  $n_{\text{H}} = 1.5\text{--}1.9\text{ cm}^{-3}$ ) nearly radially away from us. Moreover, even higher spatial-resolution images of *Herschel* resolved the arc into multiple pieces, allowing Decin et al. (2012) to conclude that the giant convection cells detected in the outer atmosphere of Betelgeuse (Kervella et al. 2011) were probably linked to localized dust creation and ejection, which eventually manifested themselves as non-homogeneous dust distributions in the split arcs and in the smaller CSEs around the central star.

For low to intermediate initial-mass stars, the trio of far-IR space telescopes were indeed used to probe the CSE in search of the onset of the axisymmetric structure development (see the next section). However, this initiative was met by a surprise. The CSE-ISM interface structure of  $\sim 200''$  radius in the far-IR was found around the AGB star, R Hya (Ueta et al. 2006; Figure 3). This structure is very much similar to the one found around Betelgeuse and other high-mass stars, albeit smaller. It was a surprise because the CSE-ISM interface structure was not expected around AGB stars. This is simply because the stellar wind velocity of AGB stars (of  $10\text{--}20\text{ km s}^{-1}$ ) was in general considered too low to cause shocks and active interactions at the CSE-ISM interface. Actually, what matters in such circumstances is the *relative* velocity of the stellar wind with respect to the local ISM. Hence, if there is *relative* motion between the star and the local ISM (i.e., the local ISM moves with respect to the star or the star moves with respect to the local ISM, or both), the *relative* wind velocity (i.e., the intrinsic wind velocity,  $v_*$ , plus the space velocity of the star relative to the local ISM,  $v_{*,\text{ISM}}$ ) can be high enough to form a steady stellar wind bow shock structure. In retrospect, the stellar wind bow shock of Betelgeuse does correspond exactly to the case where the sizable local ISM flow enhances the *relative* motion of the star with respect to the local ISM even when the wind velocity is relatively low (Ueta et al. 2009; Ueta 2011).

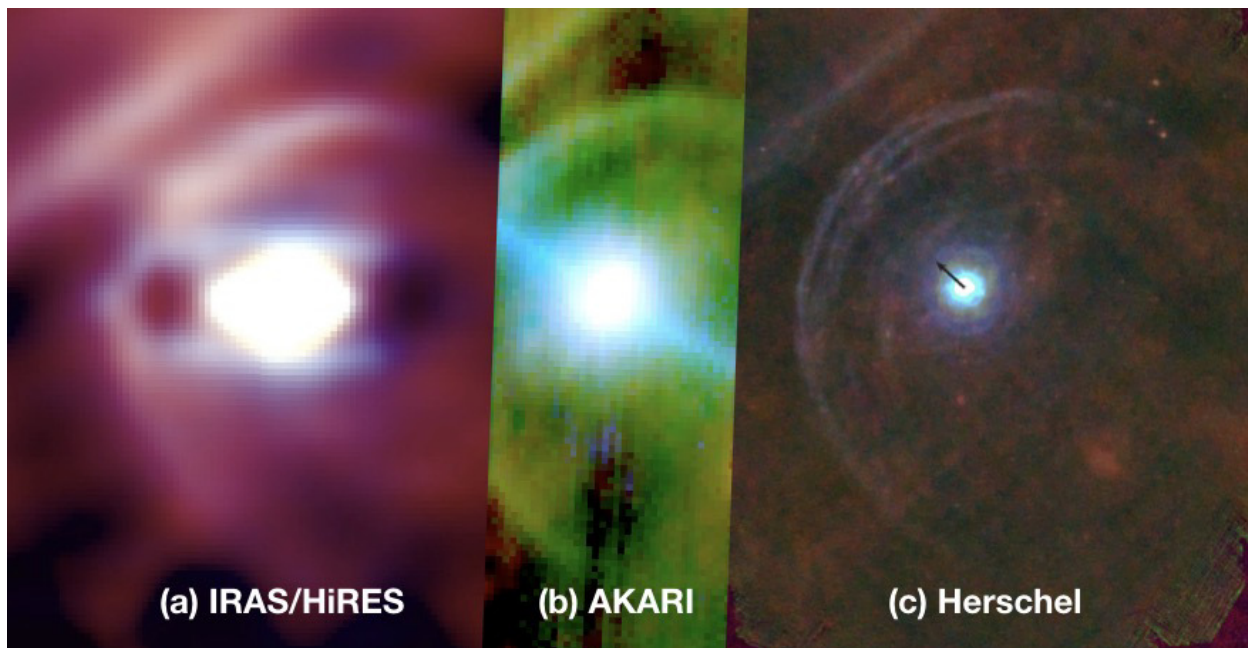


**Figure 2.** The CSE-ISM interface region around Betelgeuse (the arc structure having  $6'$  to  $7'$  radius) captured in the far-IR over the course of roughly 25 yrs. (a) *IRAS/HiRES* image at roughly  $1'$  resolution ( $60$  and  $100\ \mu\text{m}$  blue/red composite; Noriega-Crespo et al. 1997b). (b) *AKARI* image at about  $30''$  resolution ( $65$ ,  $90$ ,  $140\ \mu\text{m}$  blue/green/red composite; only the central region was scan-mapped; Ueta et al. 2008). (c) *Herschel* image at nearly  $8''$  resolution ( $70$ ,  $100$ ,  $160\ \mu\text{m}$  blue/green/red composite; Decin et al. 2012). North is up, and E to the left.

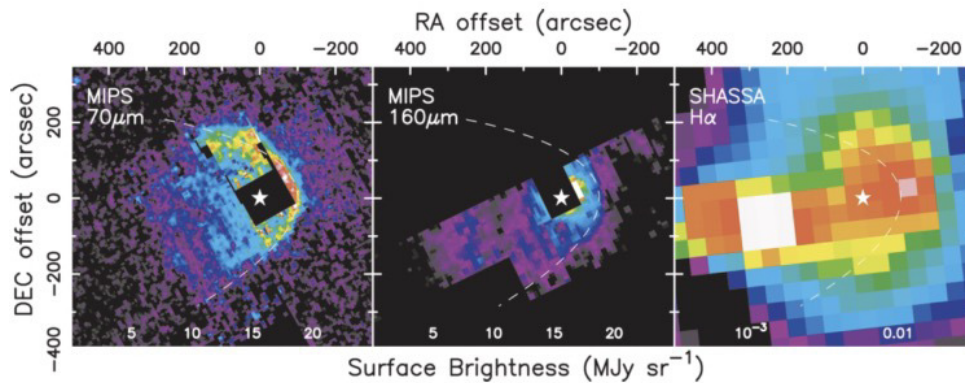


**Figure 3.** PSF-subtracted *Spitzer*/MIPS maps of R Hya at  $70\ \mu\text{m}$  (left) and  $160\ \mu\text{m}$  (middle), with a SHASSA  $\text{H}\alpha$  map (right; Gaustad et al. 2001) for comparison. The position of the star is indicated by the star symbol. The tick marks indicate the angular offsets in arcseconds. Linear color scaling of surface brightness (in  $\text{MJy sr}^{-1}$ ) is shown at the bottom of each panel. A parabolic curve  $y = x^2/3l$ , which closely represents the stellar wind bow shock near the apex, is displayed by the dashed lines. North is up, and E to the left. Adopted from Ueta et al. (2006).

*AKARI* observations subsequently found two resolved cases of the CSE-ISM interactions around the AGB stars, R Cas (Ueta et al. 2010; Figure 4, left) and U Hya (Izumiura et al. 2011; Figure 4, right). In the case of R Cas, the characteristic stellar wind bow shock structure was found after the point-spread-function (PSF) of the central star was mitigated by deconvolution. However, the case of R Cas was found to be somewhat different from that of R Hya because the shape of the arc structure is fairly circular (eccentricity is 0.3) and the relative position of the central star with respect to the central star is fairly close to the center of the rather circular arc structure (Ueta et al. 2010). The case of U Hya was found to be even more different, because its *AKARI* maps showed the ring-like CSE that was interpreted as the result of the previous mass loss enhancement caused by the last thermal pulse event. Still, there was some excess emission extended radially into a particular direction beyond the ring structure, attributed to the circumstellar matter being blown-off from the ring-like CSE via interactions with the ISM (Izumiura et al. 2011, their Figure 8).

*Herschel* followed suit to observe about 70 CSEs of evolved stars (via the Mass-loss of Evolved StarS, or MESS, guaranteed time key program; Groenewegen et al. 2011). While the original objective of the MESS program was to probe the CSE to trace the AGB mass loss history, Cox et al. (2012) found the stellar wind bow shock and related structures in a significant fraction (50 out of 78, or 63%) of the AGB stars and red supergiant in the MESS sample: the detection rate improved to 43 out of 56, or 78%, if the sample was restricted to only nearby objects ( $D \leq 500\ \text{pc}$ ) to reduce observational uncertainties. These numbers are also corroborated by the MLHES (excavating Mass Loss History in extended dust shells of Evolved Stars) mission program of *AKARI* with the sample of 144 AGB stars and related objects (Ueta et al. 2007; Ueta et al. in preparation). *Herschel* achieved by far the highest spatial resolution and was able to resolve internal structures within the stellar wind bow shock structure that were thought to arise due to instabilities (Jorissen et al. 2011).

In this way, the original discovery of the AGB CSE-ISM interaction case around R Hya by *Spitzer* was followed through by *AKARI* and *Herschel* surveys to conclude that these CSE-ISM interaction cases are rather ubiquitous. These observational findings also prompted a number of numerical investigations into AGB CSE-ISM interactions (e.g., Wareing et al. 2006; Mohamed et al. 2012; van Marle & Keppens 2012; van Marle et al. 2014). However, we are not yet certain why the CSE-ISM interface region is bright in the far-IR, even though we have always naively referred to it as the stellar wind bow shock. At the CSE-ISM interface, there would be a pile-up of the circumstellar and interstellar matter. If there are shock interactions at the interface, these shocks can induce collisionally excited line emission ( $\text{H}\alpha$  is hinted at for the R Hya case as seen in the SHASSA  $\text{H}\alpha$  map; Figure 3, right). If this is the case, far-IR fine-structure lines can potentially boost the far-IR broadband fluxes of the region. Even if shocks are absent, the interstellar radiation field can penetrate into the CSE-ISM interface region from outside and can raise the temperature of the region to 20 to 40 K. Then, together with the column density enhancement at the CSE-ISM interface due to the material pile-up, far-IR continuum fluxes from the interface could be strengthened.

Attempts were made to obtain IR spectra from the CSE-ISM interface region around R Hya using *Spitzer*. However, no emission lines were positively detected in the 20 and  $80\ \mu\text{m}$  bands even when the enormously bright and extensive central star's PSF spider structures fell onto the slit placed across the CSE-ISM interface region. This suggested that the far-IR emission in the CSE-ISM interface region was largely thermal dust emission. Unfortunately, the far-IR surface brightness in any of the CSE-ISM interface regions discovered was too low for *Herschel*/PACS to make reasonable detections (about  $1\ \sigma$  detection would be achieved with the maximum integration of 8 hr). Therefore, this issue will have to wait for the future generation of far-IR observatories, which will offer greater surface brightness sensitivities in spectroscopic observations. The absence or presence of shock interactions could have significant implications in terms of the chemical evolution of the ISM, because the answer to this unresolved question will most likely settle whether or not the CSE material is processed for the last time when it gets incorporated into the ISM.

In the mean time, it is prudent to perform new far-IR unbiased searches for these CSE-ISM interaction regions using data from the *AKARI* far-IR all-sky survey (Doi et al. 2015), the *Spitzer* inner Galactic plane survey (Carey et al. 2009) and the *Herschel* infrared Galactic plane survey (Molinari et al. 2010), as has been done with the *Spitzer* 24  $\mu\text{m}$  data to catalog extended disk- and ring-like objects (Mizuno et al. 2010).

### 3. THE DENSITY DISTRIBUTIONS IN THE EXTENDED CSES

At the same time, a number of programs were executed to address the issue of AGB mass loss by mapping the density distributions in the extended CSEs, aiming to capture the onset of the axisymmetric structure development. These programs include MIRIAD (MIPS Infrared Imaging of AGB Dustshells; PI: A. K. Speck; Ueta et al. 2006; Izumiura et al. 2011), COASTING (PI: M. Morris; Do et al. 2007), and *Spitzer*-MLHES (PI: T. Ueta; Ueta et al. 2010) using *Spitzer*, MLHES (PI: I. Yamamura; Ueta et al. 2010; Izumiura et al. 2011; Ueta 2011; Ueta et al. 2017) and FISPAN (PI: P. García-Lario; Cox et al. 2011) using *AKARI*, and MESS (PI: M. A. T. Groenewegen; e.g., Groenewegen et al. 2011) and HerPlaNS (*Herschel* Planetary Nebula Survey; PI: T. Ueta; Ueta et al. 2014; Otsuka et al. 2017) using *Herschel*.

Unfortunately, mapping extended CSEs with *Spitzer* turned out to be challenging because (1) a significant portion of the MIPS 70 and 160  $\mu\text{m}$  arrays were lost during launch and (2) the central star had to be avoided to prevent the MIPS 24  $\mu\text{m}$  array from saturating (even when the 24  $\mu\text{m}$  data were not needed). Nevertheless, both of the MIRIAD and *Spitzer*-MLHES programs yielded a certain amount of results: the discovery of the CSE-ISM interface in R Hya was made (Ueta et al. 2006), and other peculiar CSE-ISM interface cases were studied (Ueta et al. 2010; Izumiura et al. 2011). However, because *Spitzer* CSE maps usually lack the central 50''  $\times$  100'' region (e.g., Figure 3), the latest mass loss history cannot be learned effectively from these maps.

*AKARI* slow-scan maps achieved the  $1\sigma$  sensitivity of slightly less than 1  $\text{MJy sr}^{-1}$ , thanks to the slow scan-mapping speed at 8'' or 15''  $\text{s}^{-1}$ , its cooled mirror, and marginal spatial resolution. Hence, *AKARI* CSE maps attained by far the greatest sensitivities among far-IR images produced by the trio of far-IR space telescopes. The *AKARI* MLHES mission program was designed to address specifically the AGB mass loss by understanding the density distributions in the evolved star CSEs via the far-IR mapping of cold thermal dust emission in 144 AGB stars and other types of evolved stars (Ueta et al. 2007). The gist of the aim of the program was already established by Izumiura et al. (2011) in their investigations into the density distributions in the CSE of the AGB star, U Hya (Figure 4, right). After removing the PSF effects due to the central star by subtracting a scaled image of a reference point source, the CSE-only maps, in which a detached CSE was revealed, were generated. The radial profiles were carefully examined to determine if the detached CSE was caused by (1) the temporal enhancement of mass loss due to thermal pulse and the subsequent two-wind interactions or (2) the reverse/termination shock of the stellar wind bounced back from the CSE-ISM interface. While the former scenario was likely and preferred, the latter scenario was not completely refuted by the presence of the cometary tail structure seen (Figure 8 in Izumiura et al. 2011) and the marginal spatial resolution of the CSE-only images that did not allow a decisive determination of the more likely scenario.

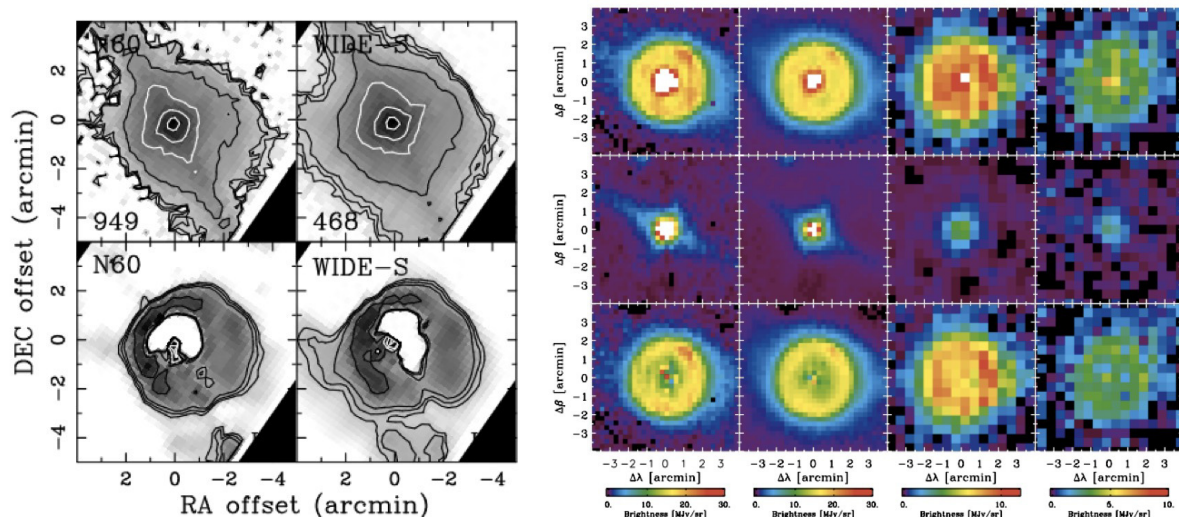


**Figure 4.** [Left]: *AKARI* maps of R Cas in the N60 (65  $\mu\text{m}$ ) and WIDE-S (90  $\mu\text{m}$ ) bands at 15''  $\text{pix}^{-1}$  scale (top panels). The number at the bottom left indicates the peak surface brightness in  $\text{MJy sr}^{-1}$ . The central star is still bright and suffers from the linear cross-talk artifact, which hides much of the CSE structures. The corresponding deconvolved maps using the Lucy-Richardson algorithms are also shown (bottom frames). N is up, and E to the left, with RA and Dec offsets. Adopted from Ueta et al. (2010). [Right]: *AKARI* images of U Hya (top) and a point source (middle), and the point-source-subtracted maps (bottom) at 65, 90, 140, and 160  $\mu\text{m}$ . The color wedge at the bottom indicates the surface brightness in  $\text{MJy sr}^{-1}$ . Each panel is 8''  $\times$  8''. Ecliptic north is up, and ecliptic east to the left. Equatorial north is tilted at  $-23.4^\circ$ . Taken from Izumiura et al. (2011).

Meanwhile, *AKARI* slow-scan maps were known to have been affected by the slow transient effects of the Ge:Ga arrays used for *AKARI*'s far-IR instrument, which would manifest as underestimates of the surface brightness especially when bright targets are scanned over. Shirahata et al. (2009) presented a method to correct for point-source fluxes. However, it was not clear if marginally extended bright sources would need a correction for their surface brightness. Ueta et al. (2017) have recently established a procedure to correct slow-scan maps directly and recover the true far-IR surface brightnesses based on the empirical power-law detector response function, adopted from the observed scale invariant characteristics of slow-scan maps (i.e., PSF shapes remain the same irrespective of the PSF brightness). With this surface brightness correction method established, the rest of the MLHES sample is being examined presently to be reported momentarily.

The MESS program was the major survey of the evolved star CSEs with *Herschel*. The power of its unprecedented spatial resolution was already seen in the previous section in revealing the split stellar wind bow shock structure in Betelgeuse (Decin et al. 2012; Figure 2) and discovering a number of CSE-ISM interaction cases in the sample (Cox et al. 2012). The resolving power of *Herschel* was proven effective again in studying the CSE structures of the MESS sample more closely. Following the discovery of the spiral structures due to mass loss modulations of the central binary system in CO (Maercker et al. 2012), Mayer et al. (2013, 2014) found internal spiral structures in the far-IR CSE characteristic to mass loss modulations of the central binary system (Figure 5, left).

There was also the HerPlaNS program, aimed at mapping a handful of planetary nebulae simultaneously in thermal dust continuum and fine-structure lines in the far-IR (Ueta et al. 2014). The unprecedented spatial resolution of *Herschel* revealed the distributions of thermal dust continuum emission very similar to those of emission lines in the optical and the distributions of fine-structure line emission that are very distinct depending on the degree of excitation (Figure 5, middle, for NGC 6781). Combined with the existing panchromatic data from X-ray to radio, Otsuka et al. (2017) performed detailed analyses of the properties of one of the HerPlaNS targets, NGC 6781 (plasma diagnostics, abundance analyses (Figure 5, right), and fitting of the luminosity and distance of the central star) and used the results of these analyses as input parameters to derive the best-fit dusty photo-ionization model using the CLOUDY code (Ferland et al. 2013). They found that the ionized part of the nebula was only a small fraction ( $\sim 20\%$ ) of the entire CSE (i.e., the bulk of the nebula turned out to be the photo-dissociation region) and that the observed nebula accounted for about 70% of the mass theoretically predicted to have been ejected during the final thermal pulse event by the  $2.25\text{--}3.0 M_{\odot}$  initial-mass progenitor star of NGC 6781 (as concluded from the abundance analyses compared with AGB nucleosynthesis models by Karakas 2010). The HerPlaNS work is now expanded to include all PNe observed by *Herschel* (K. Asano, *in preparation*).

There were programs aimed at observing PPNe in the far-IR that are transitioning from AGB stars to PNe. As shown by Do et al. (2007) and Cox et al. (2011), the extended part of the CSE was not detected in the far-IR most likely because (1) the central star that is not yet hot enough (i.e., the CSE is not yet ionized in the PPN phase), and (2) the CSE is still expanding (i.e., the bulk of the circumstellar matter is still found in the inner CSE). Hence, there is not yet any appreciable amount of far-IR surface brightness from the CSE during the PPN phase, even though the inner CSE emits a reasonable amount of mid-IR surface brightnesses (e.g., Meixner et al. 1999; Lagadec et al. 2011).

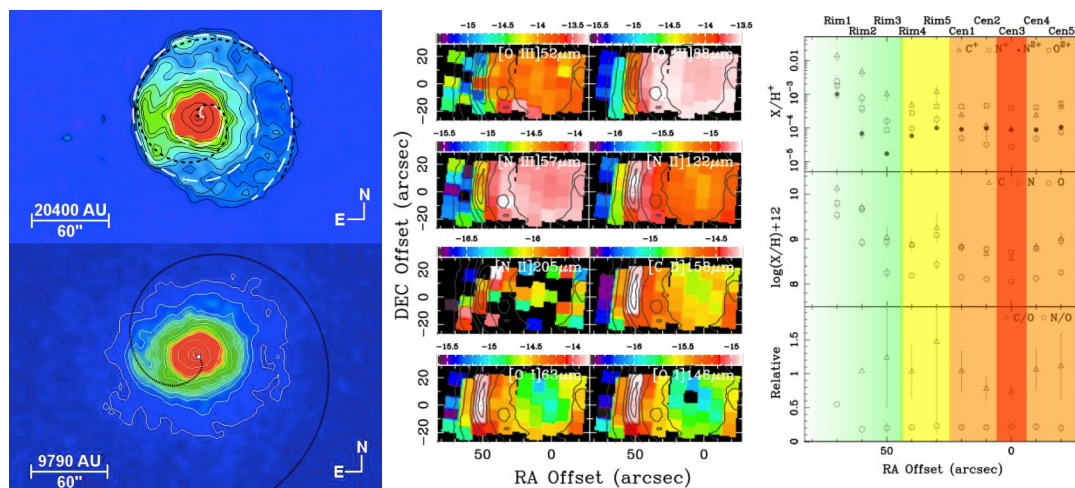


**Figure 5.** [Left] [Top] Contour plot of the deconvolved  $70\ \mu\text{m}$  *Herschel* image of W Aql, revealing two Archimedean spirals with a separation distance of  $52''$  (black) and  $26''$  (white). Taken from Mayer et al. (2013) [Bottom] Contour plot of the *Herschel*  $70\ \mu\text{m}$  image of  $\pi^1$  Gru overlaid with an Archimedean spiral with a  $116''$  spacing of the known G0V companion. Taken from Mayer et al. (2014). [Middle] *Herschel* line maps in color overlaid with  $70\ \mu\text{m}$  contours, covering the central  $111'' \times 56''$  region of NGC 6781, at [O III] $52, 88\ \mu\text{m}$ , [N III] $57\ \mu\text{m}$ , [N II] $122, 205\ \mu\text{m}$ , [C II] $158\ \mu\text{m}$ , and [O I] $63, 146\ \mu\text{m}$ . Taken from Ueta et al. (2014). [Right] Relative ionic abundance profiles (top), relative elemental abundance profiles (where  $\log N_{\text{H}} = 12$ ; middle), and C/O and N/O profiles (bottom) of NGC 6781, based on the radial plasma diagnostic and abundance analyses (Ueta et al. 2014). The nebula was sectioned into several regions of different degrees of excitation: highly ionized inner central cavity (red), ionized outer central cavity (orange), marginally ionized inner wall of the barrel structure of the nebula (yellow), and weakly ionized/PDR outer wall of the barrel structure (green).

In summary, deep far-IR imaging of the evolved star CSEs was done at  $1 \text{ MJy sr}^{-1}$  or better (especially with *AKARI* MLHES and *Herschel* HerPlaNS images) or at a few  $\text{MJy sr}^{-1}$  (most of the latest far-IR images) to empirically account for the amount of mass loss ejecta in the evolved star CSEs. The *Spitzer* discovery of the AGB CSE-ISM interface of R Hya sparked interests into the astrosphere for AGB stars and it was found to be rather universal as followed up by *AKARI* and *Herschel*. High spatial resolution images of *Herschel* characterized the inner structures within the CSE-ISM interface even when sensitivities were not  $\text{sub-MJy sr}^{-1}$ . For that matter, even  $\text{sub-MJy sr}^{-1}$  sensitivities achieved by *AKARI* and *Herschel* did not seem to have captured the CSEs in their entirety quite yet. Therefore, these lines of research will continue with the future generation of far-IR observatories having greater surface brightness sensitivities. In the mean time, it is again prudent to perform unbiased searches for the CSEs using the existing far-IR all-sky and Galactic plane survey data.

#### 4. CONCLUDING REMARKS

We have summarized stellar evolution research that has been done using far-IR data obtained with *Spitzer*, *AKARI*, and *Herschel*, especially those that aim at getting spatially-resolved images. On the one hand, we have been able to capture the evolved star CSEs in their entirety when the CSE interacts with the ISM and shows the characteristic arc-like CSE-ISM interface structure. These CSE-ISM interacting cases are found to be rather ubiquitous as long as conditions are met (i.e., there is a substantial relative motion between the mass-losing star and the local ISM), allowing us to probe the local ISM environments and stellar/ISM dynamics. However, the origin of the far-IR brightness remains unclear because of lack of direct spectroscopic data stemming from still insufficient surface brightness sensitivities in the far-IR.

On the other hand, we have not been able to capture the evolved star CSEs in their entirety when the CSE withers away into the sky background. While we have been able to achieve the  $1\text{-}\sigma$  sensitivities at a few tenth to a few  $\text{MJy sr}^{-1}$ , even these sensitivities have permitted us to capture the CSE only partially up to a fraction of the mass that has been predicted theoretically to have been ejected during the last thermal pulse event. There is a case where the observed detached shells are caused by the last two consecutive thermal pulse events. However, the detection of the outer detached shell still needs to be verified, and its origin confirmed. Even when this is true, it is still far from the original aim of these investigations—capturing the entire AGB mass loss history – because of insufficient surface brightness sensitivities in the far-IR.

Hence, there remain many questions to be answered with far-IR data at higher sensitivities in the field of stellar evolution research even when we restrict ourselves to studies based on imaging. Therefore, there is a tangible need for more sensitive observations to be carried out with future instruments aboard the *SOFIA* (*Stratospheric Observatory for Infrared Astronomy*), *SPiCA* (*Space Infrared Telescope for Cosmology and Astrophysics*), and *OST* (*Origins Space Telescope*), each of which is introduced and discussed elsewhere in this volume.

#### ACKNOWLEDGMENTS

This work is based in part on observations made with (1) the *Spitzer Space Telescope*, which is operated by the JPL/Caltech under a contract with NASA, (2) *AKARI*, a JAXA project with the participation of ESA, and (3) *Herschel*, a ESA Cornerstone Mission with significant participation by NASA. Support for this work was partially provided by an award to the original *Herschel* observing program (OT1\_tueta\_2) under RSA 1428128 issued through JPL/Caltech, and by NASA under grant NNX15AF24G issued through the Science Mission Directorate.

#### REFERENCES

- Carey, S. J., Noriega-Crespo, A., Mizuno, D. R., et al. 2009, *PASP*, 121, 76  
 Castro-Carrizo, A., Quintana-Lacaci, G., Neri, R., et al. 2010, *A&A*, 523, A59  
 Cox, N. L. J., García-Hernández, D. A., García-Lario, P., & Manchado, A. 2011, *AJ*, 141, 111  
 Cox, N. L. J., Kerschbaum, F., van Marle, A.-J., et al. 2012, *A&A*, 537, A35  
 Decin, L., Cox, N. L. J., Royer, P., et al. 2012, *A&A*, 548, A113  
 Do, T., Morris, M., Sahai, R., & Stapelfeldt, K. 2007, *AJ*, 134, 1419  
 Doi, Y., Takita, S., Ootsubo, T., et al. 2015, *PASJ*, 67, 50  
 Ferland, G. J., Porter, R. L., van Hoof, P. A. M., et al. 2013, *RMxAA*, 49, 137  
 Gaustad, J. E., McCullough, P. R., Rosing, W., & Van Buren, D. 2001, *PASP*, 113, 1326  
 Groenewegen, M. A. T., Waelkens, C., Barlow, M. J., et al. 2011, *A&A*, 526, A162  
 Gledhill, T. M., & Yates, J. A. 2003, *MNRAS*, 343, 880  
 Hacking, P., Neugebauer, G., Emerson, J., et al. 1985, *PASP*, 97, 616  
 Harper, G. M., Brown, A., & Guinan, E. F. 2008, *AJ*, 135, 1430  
 Hashimoto, O., & Izumiura, H. 1998, *Ap&SS*, 255, 349  
 Hashimoto, O., Izumiura, H., Kester, D. J. M., & Bontekoe, T. R. 1998, *A&A*, 329, 213  
 Hawkins, G. W., & Zuckerman, B. 1991, *ApJ*, 374, 227  
 Herwig, F. 2005, *ARA&A*, 43, 435  
 Iben, I., Jr. 1981, *ApJ*, 246, 278  
 Iben, I., Jr. 2012, *Stellar Evolution Physics 2-Volume Set* (Cambridge: Cambridge University Press)  
 Izumiura, H., & Hashimoto, O. 1998, *Ap&SS*, 255, 341

- Izumiura, H., Hashimoto, O., Kawara, K., Yamamura, I., & Waters, L. B. F. M. 1996, *A&A*, 315, L221
- Izumiura, H., Ueta, T., Yamamura, I., et al. 2011, *A&A*, 528, A29
- Izumiura, H., Waters, L. B. F. M., de Jong, T., et al. 1997, *A&A*, 323, 449
- Jorissen, A., Mayer, A., van Eck, S., et al. 2011, *A&A*, 532, A135
- Kessler, M. F., Steinz, J. A., Anderegg, M. E., et al. 1996, *A&A*, 315, L27
- Karakas, A. I. 2010, *MNRAS*, 403, 1413
- Karakas, A. I., & Lattanzio, J. C. 2014, *PASA*, 31, e030
- Kervella, P., Perrin, G., Chiavassa, A., et al. 2011, *A&A*, 531, A117
- Knapp, G. R., & Morris, M. 1985, *ApJ*, 292, 640
- Kwok, S. 1993, *ARA&A*, 31, 63
- Lagadec, E., Verhoelst, T., Mékarnia, D., et al. 2011, *MNRAS*, 417, 32
- Maercker, M., Mohamed, S., Vlemmings, W. H. T., et al. 2012, *Nature*, 490, 232
- Mauron, N., & Huggins, P. J. 1999, *A&A*, 349, 203
- Mayer, A., Jorissen, A., Kerschbaum, F., et al. 2013, *A&A*, 549, A69
- Mayer, A., Jorissen, A., Paladini, C., et al. 2014, *A&A*, 570, A113
- Meixner, M., Campbell, M. T., Welch, W. J., & Likkell, L. 1998, *ApJ*, 509, 392
- Meixner, M., Ueta, T., Bobrowsky, M., & Speck, A. 2002, *ApJ*, 571, 936
- Meixner, M., Ueta, T., Dayal, A., et al. 1999, *ApJS*, 122, 221
- Meixner, M., Zalucha, A., Ueta, T., Fong, D., & Justtanont, K. 2004, *ApJ*, 614, 371
- Mizuno, D. R., Kraemer, K. E., Flagey, N., et al. 2010, *AJ*, 139, 1542
- Mohamed, S., Mackey, J., & Langer, N. 2012, *A&A*, 541, A1
- Molinari, S., Swinyard, B., Bally, J., et al. 2010, *PASP*, 122, 314
- Murakami, H., Baba, H., Barthel, P., et al. 2007, *PASJ*, 59, S369
- Neugebauer, G., Habing, H. J., van Duinen, R., et al. 1984, *ApJL*, 278, L1
- Noriega-Crespo, A., van Buren, D., & Dgani, R. 1997a, *AJ*, 113, 780
- Noriega-Crespo, A., van Buren, D., Cao, Y., & Dgani, R. 1997b, *AJ*, 114, 837
- Otsuka, M., Ueta, T., van Hoof, P. A. M., et al. 2017, *ApJS*, 231, 22
- Pilbratt, G. L., Riedinger, J. R., Passvogel, T., et al. 2010, *A&A*, 518, L1
- Renzini, A. 1981, *Physical Processes in Red Giants*, 88, 431
- Sahai, R., Morris, M., Sánchez Contreras, C., & Claussen, M. 2007, *AJ*, 134, 2200
- Sahai, R., Trauger, J. T., Watson, A. M., et al. 1998, *ApJ*, 493, 301
- Sedlmayr, E. 1994, *IAU Colloq. 146: Molecules in the Stellar Environment*, 428, 163
- Shirahata, M., Matsuura, S., Hasegawa, S., et al. 2009, *PASJ*, 61, 737
- Siódmiak, N., Meixner, M., Ueta, T., et al. 2008, *ApJ*, 677, 382
- Stencel, R. E., Pesce, J. E., & Hagen Bauer, W. 1988, *AJ*, 95, 141
- Ueta, T. 2002, Ph.D. Thesis, 839
- Ueta, T. 2011, *ASP Conf. Ser. 445 Why Galaxies Care about AGB Stars II: Shining Examples and Common Inhabitants* (San Francisco: ASP), 295
- Ueta, T., Meixner, M., & Bobrowsky, M. 2000, *ApJ*, 528, 861
- Ueta, T., Izumiura, H., Yamamura, I., et al. 2008, *PASJ*, 60, S407
- Ueta, T., Izumiura, H., Yamamura, I., et al. 2009, *ASP Conf. Ser. 418 AKARI, a Light to Illuminate the Misty Universe* (San Francisco: ASP), 117
- Ueta, T., Izumiura, H., Yamamura, I., et al. 2007, *AIP Conf. Proc. 948 Unsolved Problems in Stellar Physics: A Conference in Honor of Douglas Gough* (New York: AIP), 365
- Ueta, T., Ladjal, D., Exter, K. M., et al. 2014, *A&A*, 565, A36
- Ueta, T., Meixner, M., Hinz, P. M., et al. 2001, *ApJ*, 557, 831
- Ueta, T., Speck, A. K., Stencel, R. E., et al. 2006, *ApJL*, 648, L39
- Ueta, T., Stencel, R. E., Yamamura, I., et al. 2010, *A&A*, 514, A16
- Ueta, T., Tomasino, R. L., Takita, S., et al. 2017, *PASJ*, 69, 11
- van Buren, D., & McCray, R. 1988, *ApJL*, 329, L93
- van Buren, D., Noriega-Crespo, A., & Dgani, R. 1995, *AJ*, 110, 2914
- van Marle, A. J., & Keppens, R. 2012, *A&A*, 547, A3
- van Marle, A. J., Cox, N. L. J., & Decin, L. 2014, *A&A*, 570, A131
- Van Winckel, H. 2003, *ARA&A*, 41, 391
- Wareing, C. J., Zijlstra, A. A., Speck, A. K., et al. 2006, *MNRAS Letters*, 372, L63
- Waters, L. B. F. M., Loup, C., Kester, D. J. M., Bontekoe, T. R., & de Jong, T. 1994, *A&A*, 281, L1
- Werner, M. W., Roellig, T. L., Low, F. J., et al. 2004, *ApJS*, 154, 1
- Wilkin, F. P. 1996, *ApJL*, 459, L31
- Young, K., Phillips, T. G., & Knapp, G. R. 1993a, *ApJS*, 86, 517
- Young, K., Phillips, T. G., & Knapp, G. R. 1993b, *ApJ*, 409, 725